Terahertz Emission Spectroscopy of Exchange-Biased Spintronic Heterostructures: Single- and Double-Pump Techniques

Yuichi Saito,[1,*] Farhan N. Kholid,[1] Evgeny Karashtin,[2,3] Igor Pashenkin,[2] and Rostislav V. Mikhaylovskiy[1,†]

[1] *Department of Physics, Lancaster University, Lancaster LA1 4YB, United Kingdom*

[2] *Faculty of Physics, Institute for Physics of Microstructures RAS, Nizhny Novgorod, 603950, Russia*

[3] *Lobachevsky State University of Nizhny Novgorod, Nizhny Novgorod, 603950, Russia*

(Received 18 November 2022; revised 28 February 2023; accepted 9 May 2023; published 13 June 2023)

We show that terahertz (THz) emission spectroscopy is a method to probe the in-plane magnetic state in spintronic heterostructures with exchange bias between the constituent antiferromagnetic and ferromagnetic layers. We demonstrate that the intense laser excitation can switch and reversibly reset the direction of the pinning axis arising from the exchange bias in technologically relevant tunnel magnetoresistance elements. By applying the double-pump THz emission spectroscopy, we reveal that this switching exhibits a threshold character in the pump intensity.

DOI: 10.1103/PhysRevApplied.19.064040

I. INTRODUCTION

Antiferromagnets, materials with antiparallel spin alignment, encompass the largest class of magnetic materials. They have become relevant in spintronic applications since the discovery of exchange bias [1]. When an antiferromagnet is adjacent to a ferromagnet, exchange coupling between spins of both magnetic phases induces a preferential direction of the ferromagnetic magnetization, or unidirectional anisotropy, and an increase in coercivity [2,3]. The lateral shift and widening of the hysteresis loop of a ferromagnet are particularly useful in spin-valve and tunneling magnetoresistance (TMR) heterostructures, where the electrical resistance of the device can be controlled via the relative orientation of two ferromagnetic layers separated by a nonmagnetic metallic layer [4] or an insulating layer [5,6]. Implementing the exchange bias enables a range of applied magnetic fields, in which the two ferromagnetic layers are antiparallel relative to each other, as one interacting with the antiferromagnet requires a stronger field to switch, which is advantageous for device applications.

With interest in understanding the fundamental limit of magnetization reversal, exchange-bias structures were also investigated using ultrafast pump-probe spectroscopy by Ju *et al.* [7,8], in which an intense laser pulse created a nonequilibrium state of electrons in the magnetic metals and another weaker pulse interrogated the time evolution of this state [9]. Laser-pulse perturbation is found to modify the exchange bias, as evidenced by the distortion of the hysteresis loop observed by the magneto-optic Kerr effect (MOKE) with a fixed time delay after strong laser-pulse excitation. Subsequent studies confirmed this by observing ferromagnetic precession in the time domain after laser-pump excitation [10–13]. The transient reduction of exchange bias alters the effective field applied to the ferromagnet, and consequently, magnetization undergoes precession along the new equilibrium axis.

However, the all-optical pump-probe method is not free from nonmagnetic artifacts, such as the state-filling effect [14] and the laser-induced reflectivity change [15], and in the case of metallic heterostructures, the interpretation of signals can be ambiguous [15]. Thus, an alternative experimental technique, terahertz (THz) emission spectroscopy, emerged in the past decade as a prominent tool for various ultrafast magnetism studies [16,17], opening the subfield of THz spintronics [18,19]. This method can replicate spin-transport effects using the exact same spintronic heterostructures as in transport electrical methods, while having a much shorter time resolution and, at the same time, preventing magneto-optical artifacts.

Recently, Wu *et al.* reported terahertz emission from exchange-biased samples to demonstrate field-free emitters from a practical point of view [20], although they did not discuss the dynamics of the exchange bias itself. In this study, we investigate the laser-induced

*y.saito@lancaster.ac.uk

†r.mikhaylovskiy@lancaster.ac.uk

dynamics of exchange bias at an IrMn/CoFeB interface at ultrafast timescales using terahertz emission spectroscopy [Fig. 1(a)]. First, we confirm that under the low-fluence-excitation regime the THz emission reveals the hysteresis corresponding to the exchange bias. Then we observe that increasing fluence leads to weakening and eventual destruction of the exchange bias. Nonetheless, by applying the bias magnetic field during and after laser illumination, we can restore the exchange bias and reset its direction. To further investigate the laser-induced change of the exchange bias, we employ double-pump spectroscopy, which is recently used for the nonlinearity [21] and phase transition in FeRh [22,23]. In this way, we observe that the destruction of the exchange bias has an optical intensity threshold. We also verify that the observed effects can be achieved in an archetypical magnetic-tunnel-junction heterostructure.

II. SAMPLES

To investigate THz emission from spintronic structures with exchange bias, we prepare two different types of samples (we used $Co_{40}Fe_{40}B_{20}$ and $Ir_{20}Mn_{80}$ for all samples): Ta(10)/IrMn(10)/CoFeB(4)/Ta(5), with one ferromagnetic layer, and Ta(10)/IrMn(10)/CoFeB(4)/MgO(1.5)/CoFeB(4)/NM(x), with two ferromagnetic layers, i.e., a magnetic tunnel junction (MTJ), as shown in Fig. 1(b) (thicknesses are given in nm). In this paper, we call them type 1 and type 2, respectively. For a nonmagnetic (NM) layer, we select Ta and Pt, which are broadly used in spintronics. IrMn is also a widely used antiferromagnet because of the advantages of a high Néel temperature (T_N) and blocking temperature (T_B). Typical values are $T_N = 721$ K for the bulk γ phase [24] and $T_B = 500$ K for the $Ir_{19}Mn_{81}(10)/Co_{90}Fe_{10}(20)$ bilayer [25]. The Ta layer under IrMn is inserted mainly for better adhesion.

Both structures are grown on quartz substrates by magnetron sputtering. The base pressure in the chamber does not exceed 3×10^{-7} Torr. The working argon pressure during growth of Ta, CoFeB, and Pt is 2 mTorr and during growth of IrMn is 4 mTorr. The MgO layer is formed by rf magnetron sputtering of the dielectric stoichiometric MgO target at 1.5 mTorr. Structure growth is carried out under an external magnetic field of 170 Oe applied in the in-plane direction of the wafer.

The hysteresis loops of each sample along their pinning axes are measured magneto-optically [they are shown as blue broken lines in Figs. 3(b) and 6]. One can see that a single CoFeB layer grown on an IrMn antiferromagnet has well-induced exchange bias. In contrast, we can evidently switch this system between the parallel and antiparallel states by applying a small magnetic field along the pinning axis.

III. SINGLE-PUMP THz EMISSION

A. Method

We employ a femtosecond Ti:sapphire laser with a regenerative optical amplifier with a pulse width and central wavelength of 40 fs and 800 nm, respectively. A linearly polarized pump beam is directed onto the substrate side of the sample, generating the radiation of the THz pulse. The pump spot is loosely focused with a lens onto the sample position. We confirm that the waveforms of THz emission are independent of the pump polarization, both different angles and circular ones.

As shown in Fig. 1(a), the laser pulse hitting the sample excites a spin-polarized current, j_s, in the FM layer arising from hot electrons in the different densities of states between up and down spins. The spin current propagates from the FM layer to an NM layer, which is converted into

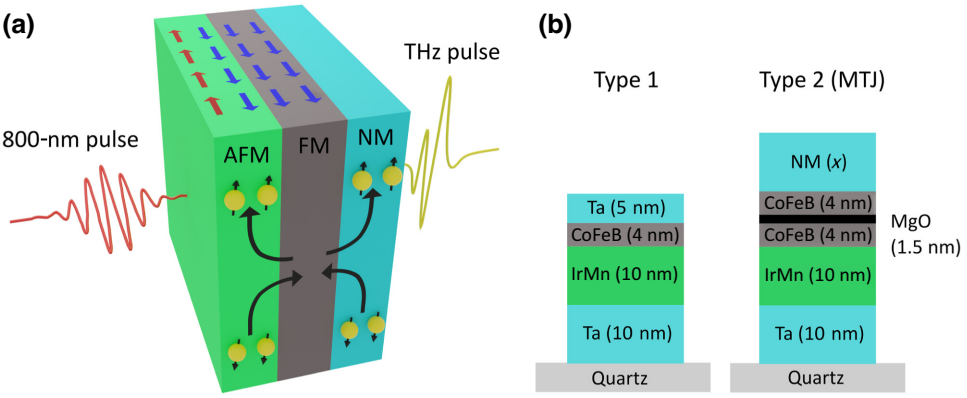

FIG. 1. (a) Mechanism of terahertz emission from the spintronic emitter with exchange bias. Photoexcited spin current, illustrated by black arrows, propagates from the ferromagnet (FM) layer into both NM and antiferromagnet (AFM) layers and is converted into charge current via the inverse spin Hall effect. (b) Sample structures fabricated by sputtering. Type 1 has only one FM layer, CoFeB, with an AFM layer, IrMn, for the exchange bias, while type 2 has two FM layers insulated by MgO, a so-called MTJ. Only the bottom CoFeB (pinned layer) is exchange biased by adjacent IrMn, while the upper layer is a free layer.

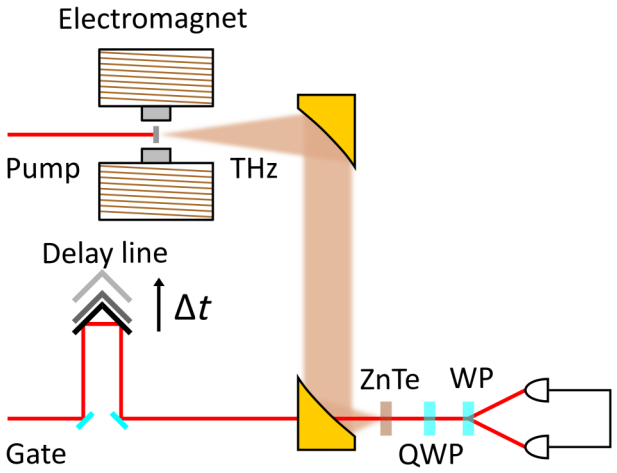

FIG. 2. Schematic of the single-pump measurement setup. Set of gold-coated parabolic mirrors guide the terahertz pulse to the ZnTe crystal. Electromagnet provides a magnetic field in the plane of the sample. Quarter-wave plate (QWP) balances the static signal and a Wollaston prism (WP) splits the gate into *s* and *p* polarization, which are detected with a balanced photodetector. We define Δt as the delay time between pump and gate.

an electric field (a charge current) if the neighboring NM layer has a spin Hall angle, θ_{SH}. The THz inverse spin Hall effect (ISHE) can be expressed as [26]

$$\mathbf{E}_{\mathrm{THz}} \propto \theta_{\mathrm{SH}}\, \mathbf{j}_s \times \boldsymbol{\sigma}, \tag{1}$$

which is simplified with the exact tensor formula. The spin polarization, $\boldsymbol{\sigma}$, is dependent on the magnetization of the FM layer, the magnitude and polarity of which correspond to the amplitude and polarization of the THz electric field, $\mathbf{E}_{\mathrm{THz}}$. Notably, the samples we measure contain a metallic AFM layer, IrMn, which also has a nonzero θ_{SH}. Thus, for the type 1 sample, the spin current, $\mathbf{j}_s$, flows and is injected into both IrMn and Ta layers in the opposite direction. However, the IrMn and Ta layers have positive and negative θ_{SH}, that is, opposite signs as well. Consequently, the THz emission from the two layers is enhanced in phase [20]. According to a previous report, the decay length of the spin current in IrMn is approximately 0.5 nm in the terahertz-frequency range [27]. This shorter length, compared to our IrMn thickness, indicates that the base Ta(10) layer is negligible for THz emission via the ISHE. Moreover, the polarity is flipped when we measure the waveform, where the pump pulse is directed from the opposite side. It means the other emission mechanism of a magnetic dipole can be neglected in this sample, which is consistent with previous reports [20,21].

To measure emitted THz waveforms by electro-optic (EO) sampling, a sufficiently weak pulse (approximately less than 0.1% of the pump-pulse power) split from the pump line propagates in a 1-mm-thick ⟨110⟩ ZnTe crystal together with the detected THz pulse. A time delay, Δt, is controlled by a motorized stage placed on the gate beamline (Fig. 2). A quarter waveplate, a Wollaston prism, and a balanced photodetector are used to convert the optical signal into an electrical signal, which is generally called a balanced photodetection to measure the polarization ellipticity, proportional to the THz electric field. An optical chopper reduces the repetition rate of the pump from 1 kHz to 500 Hz for a lock-in-amplifier measurement.

In addition, we apply an external dc magnetic field to samples with an electromagnet, aligning the magnetization unidirectionally in plane and sweeping the field to obtain a hysteresis loop. A set of neutral density filters allows the pump power to be varied for the fluence-dependence measurement.

B. Results of type 1 (IrMn/CoFeB/Ta)

First, typical terahertz waveforms measured by EO sampling are shown in Fig. 3(a), the spectrum of which stretches up to 3 THz (limited by ZnTe detection). For all the signals, reported herein, we find no striking difference between waveforms. When fixing the delay time at the terahertz peak position and sweeping the external magnetic field, we obtain the loop depicted in Fig. 3(b). The spin current injected into the NM layer is proportional to demagnetization, and hence, initial magnetization, which is the source of the charge current emitting the terahertz pulse. In fact, the method of terahertz hysteresis reproduces the loop measured by a conventional method, magneto-optical (MO) measurement, including the shift derived from the exchange bias. We calculate the magnitude of the exchange bias (H_{EB}) and coercivity (H_c) according to the standard definition: $H_{\mathrm{EB}} = (H_{c1} + H_{c2})/2$ and $H_c = (H_{c1} - H_{c2})/2$, where H_{c1} and H_{c2} are two zero-crossing points of the hysteresis. We retrieve $H_{\mathrm{EB}} = 200$ Oe and $H_c = 260$ Oe for the MO signal, while $H_{\mathrm{EB}} = 190$ Oe and $H_c = 220$ Oe for the terahertz hysteresis. The slight discrepancy, like in a previous study [20], in these two loops probably originates from incomplete spin alignments due to the nonuniformity of the sample. Also, the penetration depth and decay depth of the spin current are critical for the detectable region in the MO signal and THz hysteresis, respectively. If the two depths are different and the sample thickness is thinner than the depths, the two loops measured with the MO signal and THz can be totally different.

We further conduct the hysteresis measurement with various pump fluences. Figure 4 shows the results for three different fluences. Although the graphs are normalized by each saturated magnetization to emphasize the difference in shape, the intensity dependence of the terahertz peak at the saturation field, $H_{\mathrm{ext}} = 1500$ Oe, is approximately proportional to the fluence, as shown in the inset of Fig. 3(a). This latter result is rather trivial and agrees with a previous report [18]. Here, we focus on the change of the

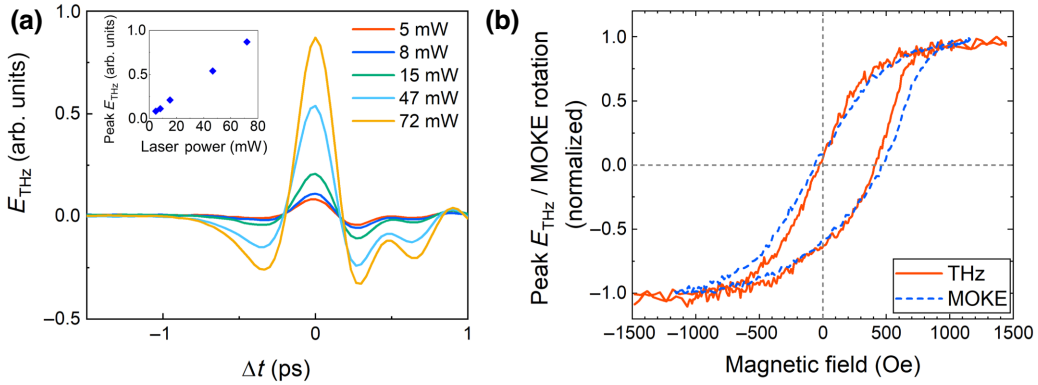

FIG. 3. (a) Typical terahertz waveforms from the type-1 sample under $H_{ext} = 1500$ Oe. Oscillation after the main peak may originate from water absorption in the atmosphere. Inset clearly shows the proportionality between the laser power (or fluence) and the terahertz peak in the region that we measure. (b) Terahertz hysteresis measured at the waveform peak (red solid line) and hysteresis measured by the magneto-optical method (blue broken line). We use 0.5 - mJ/cm^2 laser fluence for the terahertz measurement. Both data sets are normalized for easy comparison.

hysteresis loops. Measuring only with low fluence, such as 0.1 mJ/cm^2 (Fig. 4) and 0.5 mJ/cm^2 [Fig. 3(b)], we obtain the same shape as expected for the exchange bias. As the fluence increases, the hysteresis loop is distorted gradually, and finally, the coercivity and bias field almost disappear at a high fluence (4.5 mJ/cm^2). At the intermediate fluence, 2.2 mJ/cm^2, the hysteresis loop is a combined shape of the low and high fluence. It seems that this coexistence state originates from the inhomogeneous distribution of the laser fluence or nonuniformity of the sample itself, such as the magnetic domains and polycrystalline structure. The FM and AFM are completely decoupled in certain regions, while the interface exchange coupling is still in place in remaining regions.

To further elucidate the effect of high fluence, we investigate the reversibility between low and high fluences. We compare the THz hysteresis under 0.5 mJ/cm^2 illumination before and after stimulation by strong pulses of 4.5 mJ/cm^2. The exposure time under high fluence is fixed at approximately 10 s (10 000 pulses). When the external magnetic field is applied along the same direction as the exchange-bias field during exposure, the exchange bias returns to the same state as the preceding one. In contrast, the opposing polarity of the external field flips the direction of the exchange bias by the intense laser beam exposure (Fig. 5). The pinning direction can be reset with a sufficiently intense laser beam, even under a weak field of $H_{ext} = 10$ Oe. This switching shows that at high fluence the transient effective temperature at the interface exceeds the blocking temperature [28,29], and hence, CoFeB and IrMn spins are completely decoupled, and then they align with a new orientation determined by the cooling field. This result is in good agreement with a previous study on helicity-dependent optical switching of exchange [30]. Interestingly, the external field required to reset the exchange bias under laser illumination can be as small as 10 Oe, i.e., an order of magnitude smaller than that used for sample preparation. This value is consistent with the coercivity under high fluence (see inset in Fig. 4).

C. Results for sample 2 (IrMn/CoFeB/MgO/CoFeB/NM)

We repeat the measurements of the terahertz hysteresis for type 2 samples (MTJ) with two different NM layers: Pt(10) and Ta(10). To avoid heating the sample, a moderate pump fluence 0.5 mJ/cm^2 is selected. For the Pt-capped sample, as shown in Fig. 6(a), the THz hysteresis shape is totally different from that obtained from magneto-optical data and is dominated by the upper free layer, CoFeB/Pt. This agrees with the fact that Pt has a larger absolute value of spin Hall angle than IrMn. Also, the minimum signal is observed around $H_{ext} = 0$, not at a strong magnetic field of around 1500 Oe, which means the emitted THz signals from IrMn and Pt partly cancelled each other out when two layers are completely parallel. This corresponds to the same positive sign of the spin Hall angle for Pt and IrMn. For the Ta-capped sample, the hysteresis from the exchange-biased layer clearly remains in contrast to the Pt-capped one, although the polarity is inverted. This is also in agreement with comparable absolute values and the opposite sign of the spin Hall angle for IrMn and Ta (and Pt and Ta). However, in the antiparallel state around $H_{ext} = 0$, the signal is nonzero because the absolute value is greater for Ta than IrMn. Finally, we measure another sample with Ta(3)/Pt(10) for the NM layer to demonstrate the improved suppression of E_{THz} at zero magnetic field (not shown).

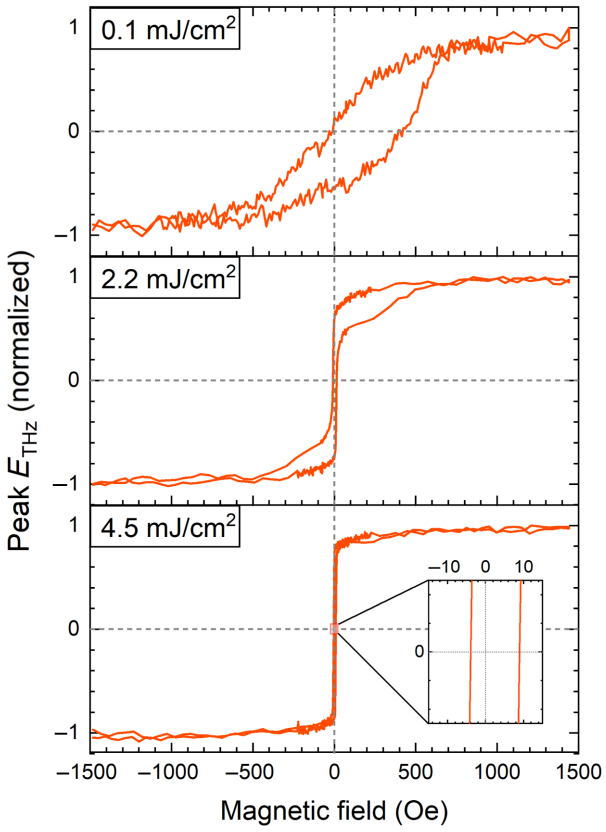

FIG. 4. Fluence dependence of the terahertz hysteresis. High-fluence (4.5 mJ/cm^2) pump eliminates coercivity and exchange, while the intermediate state is observed for 2.2 mJ/cm^2. All loops are normalized to the saturated region. Inset in the bottom graph clarifies the zero-crossing region. In addition to a low fluence of 0.1 mJ/cm^2, Fig. 2(b) also shows a similar case of low fluence, 0.5 mJ/cm^2.

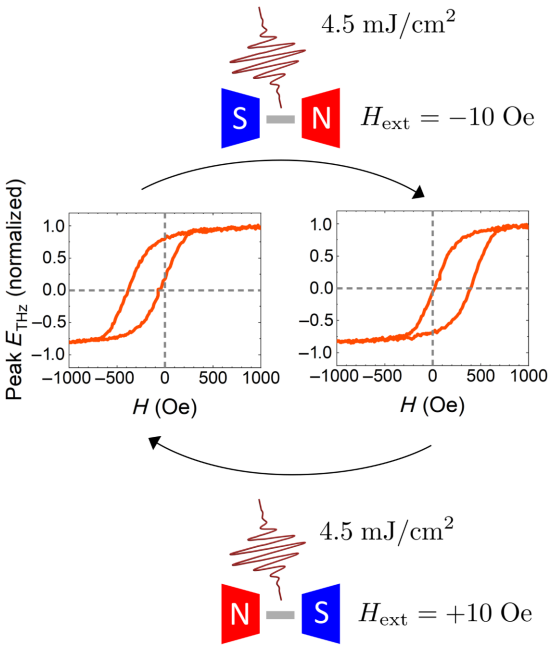

FIG. 5. Exchange-bias control in the high-fluence regime. As a result of high-fluence exposure, the exchange bias and coercivity are first totally quenched (Fig. 4), and then recover to the cooling-field-dependent direction. This reversible switching process also means we can control the orientation of exchange bias with an external magnetic field as weak as 10 Oe.

IV. DOUBLE-PUMP METHOD

A. Method

The fact that the hysteresis loops in our samples are modified by the laser pulse at high fluences poses a question regarding the origin of the bias modulation and its timescale. To explore this phenomenon of exchange-bias elimination more deeply, we carry out double-pump THz emission spectroscopy for the type 1 sample.

We depict the optical system of the double-pump terahertz emission spectroscopy in Fig. 7. The pump beam shown in Fig. 2 is split into two pump beams, named pump 1 and pump 2. Only pump 2 is modulated by the optical chopper for lock-in detection with 500 Hz. An additional delay line produces the relative time delay, $\Delta\tau$, of pump 2 with respect to pump 1. When the optical path length of pump 1 is shorter than that of pump 2, pump 1 hits the sample first and emits signal THz 1. After that, the THz 2 signal is also generated by pump 2. For the gate pulse, we fix the delay timing, Δt, at the peak of the THz 2 signal, while scanning $\Delta\tau$. As a result, we can monitor the transient phenomena on the peak amplitude of THz 2 induced by pump 1. In other words, THz 2 plays the role of a probe for optical excitation by pump 1. In the EO sampling, the contribution from THz 1 can be neglected because the repetition rate (1 kHz) is different from the lock-in reference frequency (500 Hz).

B. Results and discussion

With the double-pump setup, we trace the terahertz peak signal of pump 2 (fluence of 50 μJ/cm^2) along the time delay, $\Delta\tau$, and obtain the fingerprint of a typical ultrafast demagnetization in the FM layer [upper curve of Fig. 8(a)], which has been widely reported [31]. The higher fluence of pump 1 heats up the spin temperature more, and therefore, the demagnetization signal is remarkable in the strong pulse. The magnetization reaches almost zero with the 5 mJ/cm^2 fluence of pump 1. We increase the intensity of pump 2 to improve the signal-to-noise ratio (SNR) (0.5 mJ/cm^2) and reduce that of pump 1 (0.2 mJ/cm^2) to avoid damaging the sample [lower curve of Fig. 8(a)]. In this case, demagnetization is still seen. We select this fluence combination for the hysteresis measurement to retain a better SNR.

Next, we accumulate the terahertz hysteresis while shifting the optical delay, $\Delta\tau$ [Fig. 8(b)], and extract

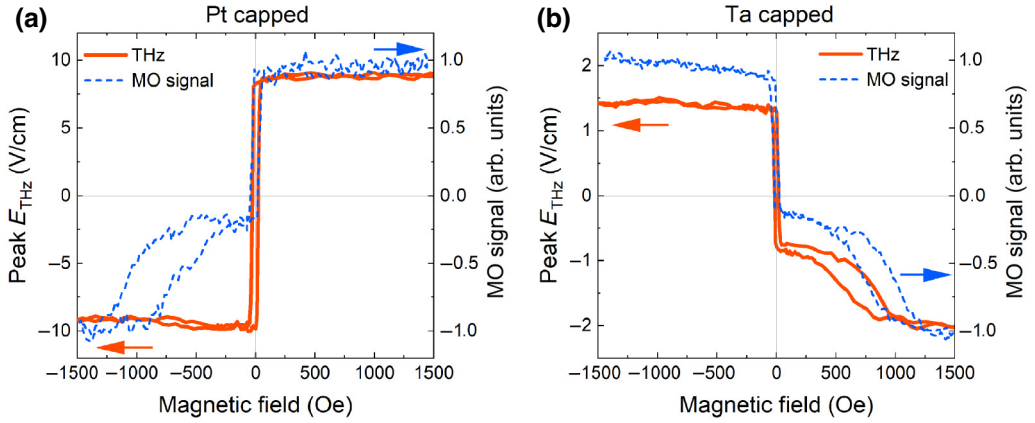

FIG. 6. Terahertz hysteresis and magneto-optical hysteresis of the MTJ sample: (a) Pt capped and (b) Ta capped. For THz hysteresis (red solid line), different magnitudes of contribution from the top and bottom FM layers is observed, especially in the Ta-capped MTJ, which has a significantly distinct loop from the magneto-optical signal (blue dashed line).

the exchange bias and coercivity from these hysteresis loop; the transient magnitude of the fields is illustrated in Fig. 8(c). As a result, we find a Gaussian-like modulation in both coercivity and bias field. At first glance, it indicates the ultrafast modulation of the exchange bias. However, Dalla Longa *et al.* pointed out [10] that the shift from one equilibrium state to another in a short time seemed unrealistic. The only way to analyze a realistic transient

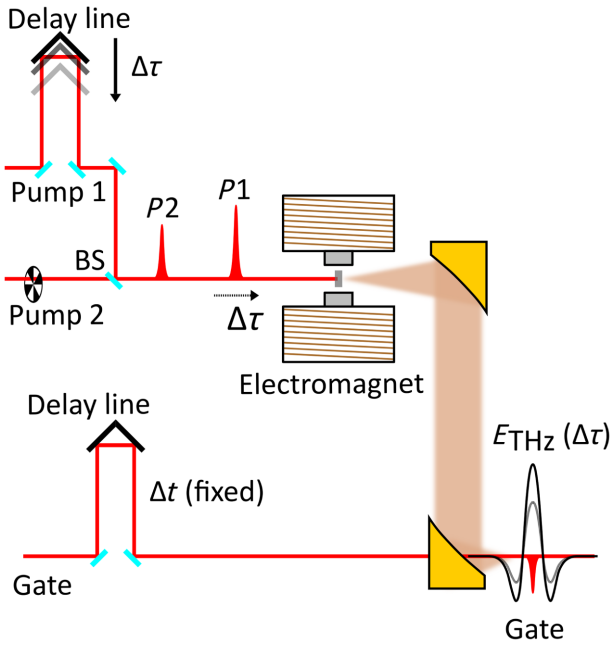

FIG. 7. Schematic of the double-pump method. Pump 1 and pump 2 excite signals THz 1 and THz 2, respectively, with a relative time delay, $\Delta\tau$, produced by an additional delay line on pump 1. Two pump beams are reunited with a 50:50 beam splitter (BS). Other delay line on the gate pulse is fixed to overlap the gate pulse with the peak of THz 2 independently of the $\Delta\tau$ scan. In terms of the EO-sampling detection, the setup is identical to that shown in Fig. 5.

change of the exchange-bias magnitude is to extract the bias field from the precession signal using the phenomenological formula, as demonstrated by Dalla Longa *et al.* However, we do not find a significant oscillation in our demagnetization signal [Fig. 8(a)] because of the noise floor or different character of magnetic anisotropy in our samples, even with longer scans. Although we cannot estimate the exchange-bias modulation in the real timescale, the Gaussian-like change of the exchange bias should be still meaningful as a clue to understand the physics.

The disappearance of exchange coupling occurs only when the two pulses overlap in time. If this effect is due to the accumulated thermal effect with multiple pulses up to the blocking temperature, the bias reduction is independent of the overlapping state ($\Delta\tau$) because the averaged power of the input laser is constant [32]. Thus, the only plausible explanation for the "ultrafast" signal on a sub-ps scale is that there exists a threshold (or strongly nonlinear behavior) in pulse intensity to alter the exchange bias and coercivity [Fig. 8(d)]. If the two pulses partially overlap or are perfectly separated, the summed intensity is not sufficient to trigger bias modulation. On the other hand, once the pulses almost overlap and the total intensity surpasses the threshold, the exchange bias and coercivity immediately get to zero. The time width of this drastic change, less than 100 fs, is in good agreement with our pulse duration, which supports our threshold scenario. In our case, the threshold fluence is in the order of 0.7 mJ/cm^2. We speculate that this intensity-origin nonlinearity originates from thermalization of the spin temperature in the AFM and FM layers. Judging from the 10% demagnetization in Fig. 8(a), we can deduce that the spin temperature in the FM layer is already increased. The blocking temperature of IrMn is lower than the Curie temperature of CoFeB, which implies that decoupling at the boundary AFM-FM interaction is possible, especially from the AFM contribution. Recently, the numerical modeling

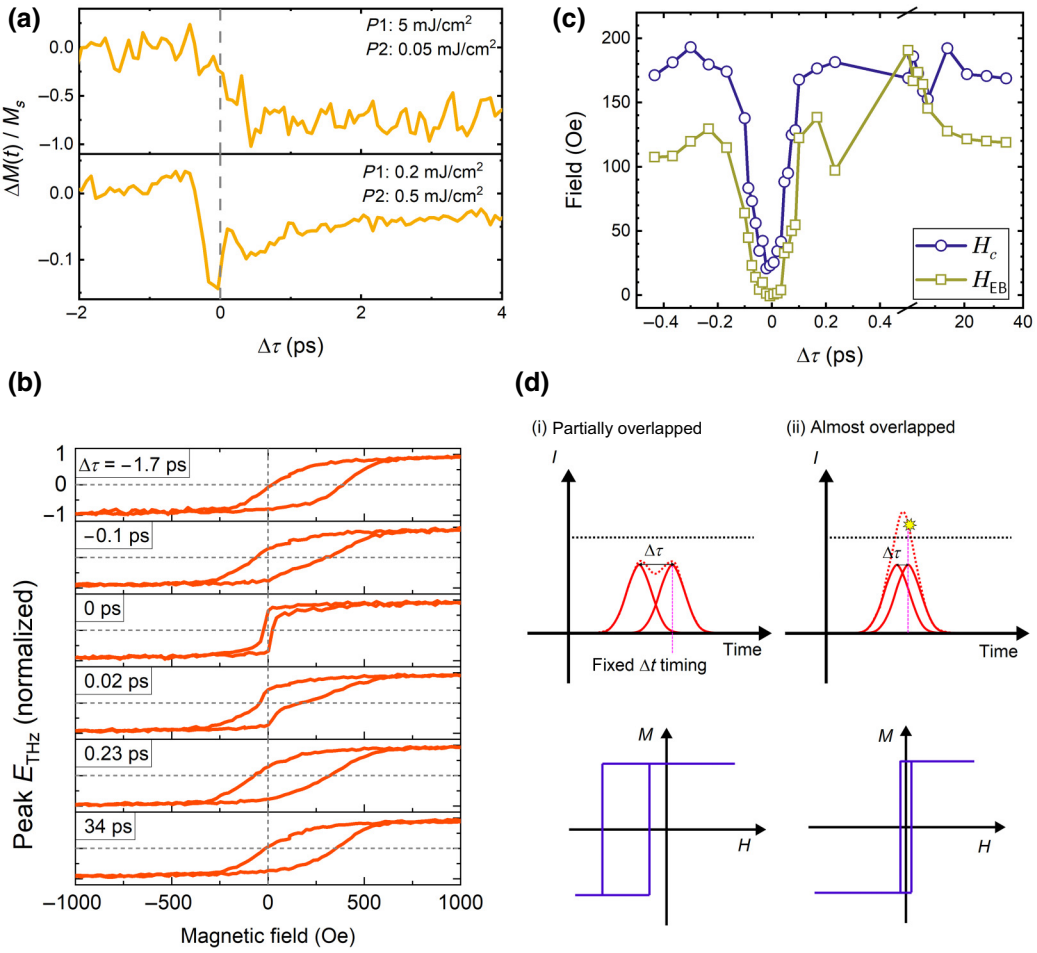

FIG. 8. (a) Tracking of the pump-2 peak in the double-pump method with different fluence combinations. Vertical scale is converted from the terahertz electric field to magnetization. (b) THz hysteresis at different $\Delta\tau$ timings. Signal magnitude is normalized for each timing. (c) Extracted exchange bias and coercivity from the series of hysteresis shown in (b). Exchange bias and coercivity show the Gaussian-like envelope at a short timescale. (d) Illustration of the threshold effect. Only when the pump pulses are close to each other is the peak intensity enhanced over the threshold. We consider that this intensity threshold triggers elimination of the exchange bias.

of demagnetization in the AFM layer manages to explain the ultrafast exchange-bias annihilation [33]. Although we cannot determine the real timescale of modulation, including the recovery time from our experimental data, their theory suggests that this phenomenon is ultrafast dynamics in an antiferromagnet.

V. CONCLUSION

We demonstrate that terahertz emission spectroscopy with a single pump is a way to measure the hysteresis loop with a remarkably high signal-to-noise ratio. The THz hysteresis exhibits a clear exchange-biased shift, even for TMR samples, in which the THz signal suffers from interference from two ferromagnetic layers, especially when their adjacent layers for the ISHE have different magnitudes of spin Hall angle. We find that the intense laser pump quenches the exchange bias, but it is restored to uniaxial bias, the orientation of which can be controlled by a weak external field. As a result of the double-pump method, we conclude that this switching effect originates from nonthermal decoupling at the antiferromagnet-ferromagnet interface. Also, the double-pump results reveal that this exchange-bias elimination has threshold behavior with respect to intensity. Our discovery may enable laser-driven magnetization switching assisted by an antiferromagnet via exchange coupling.

ACKNOWLEDGMENTS

We thank T. Mertelj and A. Fraerman for insightful discussions. This study of Y.S., F.N.K., and R.V.M. is supported by ERC Grant No. 852050 MAGSHAKE and Royal Society research Grant No. 211094. The work of E.K. is supported by the Center of Excellence "Center of Photonics" funded by the Ministry of Science and Higher Education of the Russian Federation, Contract No. 075-15-2022-316.

[1] W. H. Meiklejohn and C. P. Bean, New magnetic anisotropy, Phys. Rev. **105**, 904 (1957).

[2] J. Nogués and I. K. Schuller, Exchange bias, J. Magn. Magn. Mater. **192**, 203 (1999).

[3] R. L. Stamps, Mechanisms for exchange bias, J. Phys. D: Appl. Phys. **33**, R247 (2000).

[4] J. C. S. Kools, Exchange-biased spin-valves for magnetic storage, IEEE Trans. Magn. **32**, 3165 (1996).

[5] S. S. P. Parkin, K. P. Roche, M. G. Samant, P. M. Rice, R. B. Beyers, R. E. Scheuerlein, E. J. O'Sullivan, S. L. Brown, J. Bucchigano, D. W. Abraham, Yu Lu, M. Rooks, P. L. Trouilloud, R. A. Wanner, and W. J. Gallagher, Exchange-biased magnetic tunnel junctions and application to nonvolatile magnetic random access memory (invited), J. Appl. Phys. **85**, 5828 (1999).

[6] S. S. P. Parkin, C. Kaiser, A. Panchula, P. M. Rice, B. Hughes, M. Samant, and S.-H. Yang, Giant tunnelling magnetoresistance at room temperature with MgO (100) tunnel barriers, Nat. Mater. **3**, 862 (2004).

[7] G. Ju, A. V. Nurmikko, R. F. C. Farrow, R. F. Marks, M. J. Carey, and B. A. Gurney, Ultrafast Time Resolved Photoinduced Magnetization Rotation in a Ferromagnetic/Antiferromagnetic Exchange Coupled System, Phys. Rev. Lett. **82**, 3705 (1999).

[8] G. Ju, L. Chen, A. V. Nurmikko, R. F. C. Farrow, R. F. Marks, M. J. Carey, and B. A. Gurney, Coherent magnetization rotation induced by optical modulation in ferromagnetic/antiferromagnetic exchange-coupled bilayers, Phys. Rev. B **62**, 1171 (2000).

[9] M. C. Weber, H. Nembach, and J. Fassbender, Picosecond optical control of the magnetization in exchange biased NiFe/FeMn bilayers, J. Appl. Phys. **95**, 6613 (2004).

[10] F. Dalla Longa, J. T. Kohlhepp, W. J. M. de Jonge, and B. Koopmans, Laser-induced magnetization dynamics in CoâĹŢIrMn exchange coupled bilayers, J. Appl. Phys. **103**, 07B101 (2008).

[11] K. A. Seu and A. C. Reilly, Ultrafast laser excitation of spin waves and the permanent modification of the exchange bias interaction in IrMnâĹŢCo, J. Appl. Phys. **103**, 07C104 (2008).

[12] A. Porat, S. Bar-Ad, and I. K. Schuller, Novel laser-induced dynamics in exchange-biased systems, Europhys. Lett. **87**, 67001 (2009).

[13] F. Dalla Longa, J. T. Kohlhepp, W. J. M. de Jonge, and B. Koopmans, Resolving the genuine laser-induced ultrafast dynamics of exchange interaction in ferromagnet/antiferromagnet bilayers, Phys. Rev. B **81**, 094435 (2010).

[14] B. Koopmans, M. van Kampen, J. T. Kohlhepp, and W. J. M. de Jonge, Ultrafast Magneto-Optics in Nickel: Magnetism or Optics?, Phys. Rev. Lett. **85**, 844 (2000).

[15] R. Wilks, N. D. Hughes, and R. J. Hicken, Investigation of ultrafast spin dynamics in a Ni thin film, J. Appl. Phys. **91**, 8670 (2002).

[16] E. Beaurepaire, G. M. Turner, S. M. Harrel, M. C. Beard, J.-Y. Bigot, and C. A. Schmuttenmaer, Coherent terahertz emission from ferromagnetic films excited by femtosecond laser pulses, Appl. Phys. Lett. **84**, 3465 (2004).

[17] T. Kampfrath, K. Tanaka, and K. A. Nelson, Resonant and nonresonant control over matter and light by intense terahertz transients, Nat. Photonics **7**, 680 (2013).

[18] T. Kampfrath, M. Battiato, P. Maldonado, G. Eilers, J. Nötzold, S. Mährlein, V. Zbarsky, F. Freimuth, Y. Mokrousov, S. Blügel, M. Wolf, I. Radu, P. M. Oppeneer, and M. Münzenberg, Terahertz spin current pulses controlled by magnetic heterostructures, Nat. Nanotechnol. **8**, 256 (2013).

[19] T. J. Huisman, R. V. Mikhaylovskiy, J. D. Costa, F. Freimuth, E. Paz, J. Ventura, P. P. Freitas, S. Blügel, Y. Mokrousov, Th. Rasing, and A. V. Kimel, Femtosecond control of electric currents in metallic ferromagnetic heterostructures, Nat. Nanotechnol **11**, 455 (2016).

[20] X. Wu, H. Wang, H. Liu, Y. Wang, X. Chen, P. Chen, P. Li, X. Han, J. Miao, H. Yu, C. Wan, J. Zhao, and S. Chen, Antiferromagnetic–ferromagnetic heterostructure-based field-free terahertz emitters, Adv. Mater. **n/a**, 2204373 (2022).

[21] B. Wang, S. Shan, X. Wu, C. Wang, C. Pandey, T. Nie, W. Zhao, Y. Li, J. Miao, and L. Wang, Picosecond nonlinear spintronic dynamics investigated by terahertz emission spectroscopy, Appl. Phys. Lett. **115**, 121104 (2019).

[22] N. Awari, A. Semisalova, J.-C. Deinert, K. Lenz, J. Lindner, E. Fullerton, V. Uhlíř, J. Li, B. Clemens, R. Carley, A. Scherz, S. Kovalev, and M. Gensch, Monitoring laser-induced magnetization in FeRh by transient terahertz emission spectroscopy, Appl. Phys. Lett. **117**, 122407 (2020).

[23] G. Li, R. Medapalli, J. H. Mentink, R. V. Mikhaylovskiy, T. G. H. Blank, S. K. K. Patel, A. K. Zvezdin, T. Rasing, E. E. Fullerton, and A. V. Kimel, Ultrafast kinetics of the antiferromagnetic-ferromagnetic phase transition in FeRh, Nat. Commun. **13**, 1 (2022).

[24] T. Yamaoka, Antiferromagnetism in γ-phase Mn-Ir alloys, J. Phys. Soc. Jpn. **36**, 445 (1974).

[25] J. van Driel, F. R. de Boer, K.-M. H. Lenssen, and R. Coehoorn, Exchange biasing by $Ir_{19}Mn_{81}$: Dependence on temperature, microstructure and antiferromagnetic layer thickness, J. Appl. Phys. **88**, 975 (2000).

[26] E. Saitoh, M. Ueda, H. Miyajima, and G. Tatara, Conversion of spin current into charge current at room temperature: Inverse spin-Hall effect, Appl. Phys. Lett. **88**, 182509 (2006).

[27] O. Gueckstock, R. L. Seeger, T. S. Seifert, S. Auffret, S. Gambarelli, J. N. Kirchhof, K. I. Bolotin, V. Baltz, T. Kampfrath, and L. Nádvorník, Impact of gigahertz and terahertz transport regimes on spin propagation and conversion in the antiferromagnet IrMn, Appl. Phys. Lett. **120**, 062408 (2022).

[28] I. L. Prejbeanu, M. Kerekes, R. C. Sousa, H. Sibuet, O. Redon, B. Dieny, and J. P. Nozières, Thermally assisted MRAM, J. Phys.: Condens. Matter **19**, 165218 (2007).

[29] L. Lombard, E. Gapihan, R. C. Sousa, Y. Dahmane, Y. Conraux, C. Portemont, C. Ducruet, C. Papusoi, I. L. Prejbeanu, J. P. Nozières, B. Dieny, and A. Schuhl, IrMn and FeMn blocking temperature dependence on heating pulse width, J. Appl. Phys. **107**, 09D728 (2010).

[30] P. Vallobra, T. Fache, Y. Xu, L. Zhang, G. Malinowski, M. Hehn, J.-C. Rojas-Sánchez, E. E. Fullerton, and S. Mangin, Manipulating exchange bias using all-optical

helicity-dependent switching, Phys. Rev. B **96**, 144403 (2017).

[31] E. Beaurepaire, J.-C. Merle, A. Daunois, and J.-Y. Bigot, Ultrafast Spin Dynamics in Ferromagnetic Nickel, Phys. Rev. Lett. **76**, 4250 (1996).

[32] Q. Wu, H. Zhou, Y. Wu, L. Hu, S. Ni, Y. Tian, F. Sun, F. Zhou, X. Dong, Z. Zhao, and J. Zhao, Ultrafast quasiparticle dynamics and electron-phonon coupling in $(Li_{0.84}Fe_{0.16})OHFe_{0.98}Se$, Chin. Phys. Lett. **37**, 097802 (2020).

[33] Z. Guo, J. Wang, G. Malinowski, B. Zhang, W. Zhang, H. Wang, C. Liu, Y. Peng, P. Vallobra, Y. Xu, S. Jenkins, R. W. Chantrell, R. F. L. Evans, S. Mangin, W. Zhao, and M. Hehn, Single-shot laser-induced switching of an exchange biased antiferromagnet, arXiv:2302.04510.